

Measurements of the edge current during MAST H-modes using MSE

M.F.M. De Bock¹*; S. Saarelma¹, D. Temple¹, N.J. Conway¹,

A. Kirk¹, H. Meyer¹, C.A. Michael¹ and the MAST team¹

EURATOM/CCFE Fusion Association, Culham Science Centre, Abingdon, OX14 3DB, U.K.

Understanding ELMs is important for current and future fusion devices. ELMs are thought to be the result of peeling-ballooning modes that have a stability region determined in terms of the pressure gradient ∇p and the edge current density j_ϕ . Whereas several high resolution diagnostics exist to measure the pressure profile, j_ϕ is usually calculated using neoclassical theory. Measurements of j_ϕ would test these calculations, but are challenging in conventional tokamaks.

Motional Stark Effect diagnostics (MSE) – the most commonly used technique to derive j_ϕ in tokamaks – measure the magnetic pitch angle profile $\gamma_m = \arctan(B_\theta/B_\phi)$ which depends on the integrated current. Consequently, a change of j_ϕ in the edge will result in only a small change in γ_m , as it has to compete with the total plasma current. Moreover, MSE is dependent on the local electric field E_r as well, which can be significant in the pedestal region during H-mode. In spherical tokamaks, however, the low B_ϕ and similar B_θ , compared to conventional tokamaks, leads to a larger γ_m and also to a larger change in γ_m for any given change in j_ϕ . E.g. for a typical $B_\theta = 0.2$ T, a change $\Delta B_\theta = 0.02$ T due to an edge j_ϕ , would yield $\Delta\gamma_m = 2.8^\circ$ in a spherical tokamak with $B_\phi = 0.25$ T; whereas in a conventional tokamak with $B_\phi = 2.5$ T the change in pitch angle is only $\Delta\gamma_m = 0.46^\circ$. With a time resolution of 2 ms, the MAST MSE system (35 channels, $\sim \Delta R = 0.02$ m) can operate with a statistical error of $\sim 0.5^\circ$ in the plasma edge; enough to resolve the expected changes in γ_m [1, 2].

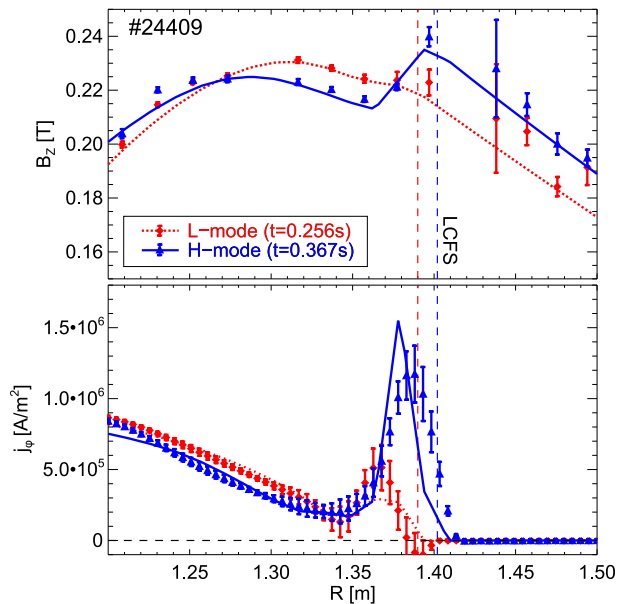


Figure 1: B_z profiles and corresponding j_ϕ for a MAST plasma in L- and H-mode directly from the MSE measurements – error bars – and from MSE constrained EFIT – lines.

*Currently at Eindhoven University of Technology, Eindhoven, the Netherlands

In MAST the MSE angle γ is measured in the mid plane ($B_R = 0, B_\theta = B_Z$) resulting in:

$$\tan(\gamma) = \frac{-\cos(\beta)B_Z - (E_r/v)\cos(\alpha + \beta)}{\sin(\alpha)B_\phi} \quad (1)$$

with β the angle between the neutral beam and the line of sight, α the angle between the toroidal direction and the neutral beam and v the beam velocity. Equation (1) is used within EFIT to constrain the equilibrium reconstruction [3]. It can, however, also be used to calculate B_Z directly from the MSE angle γ . In that case the values of B_ϕ , E_r and v are found from an initial EFIT reconstruction, the known beam energy and active Doppler spectroscopy on He^+ respectively [4]. Figure 1 shows B_Z and the corresponding j_ϕ – as derived from EFIT and directly from the MSE measurements – for L- and H-mode. The effect of E_r is reasonably small in MAST: $\sim 2\%$ in B_Z and $\sim 10\%$ in j_ϕ .

Once the B_Z profile is known, Ampère's law is used to derive j_ϕ :

$$\mu_0 j_\phi = \frac{\partial B_R}{\partial Z} - \frac{\partial B_Z}{\partial R}, \quad (2)$$

where the first term can be found from the initial EFIT reconstruction under the assumption that the flux surface shape is only weakly dependent on the local j_ϕ .

Figure 2 shows the evolution of j_ϕ , $\max(|\nabla p_e|)$ and D_α during a MAST H-mode discharge (#24409). After the L-H transition (at $t = 0.263$ s) high frequency, type III ELMs appear followed (at $t = 0.302$ s) by two long ELM free periods separated by a type I ELM at $t = 0.345$ s. A final ELM at $t = 0.392$ s terminates the H-mode. The periods around the ELMs are blocked by grey areas in figure 2 because no reliable MSE measurement exists at those times. The high frequency of the type III ELMs and the 2 ms time resolution of the MSE diagnostic meant that only a few j_ϕ profiles could be obtained during that period.

As expected one observes strong edge currents during the long ELM-free periods. The data, however, shows 2 interesting features:

- (a) Just after the ELM at $t = 0.345$ s, $\max(|\nabla p_e|)$ drops significantly, whereas $\max(j_\phi)$ keeps increasing. A possible explanation might be that current can only distribute through diffusion and hence has no time to react to the ELM.

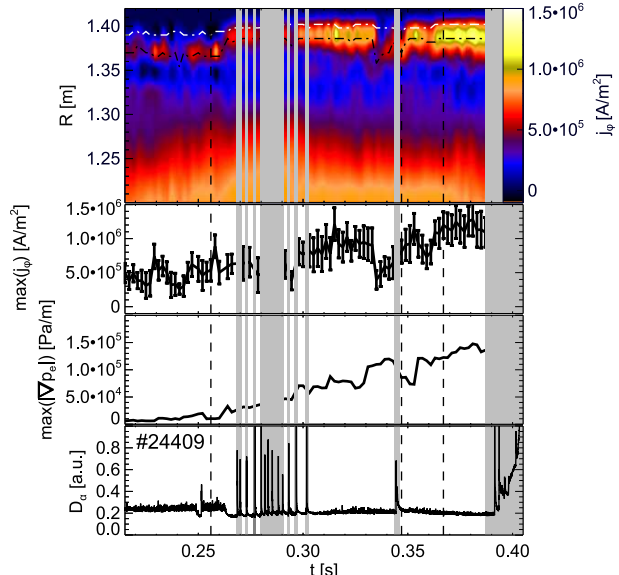


Figure 2: The evolution of j_ϕ , $\max(|\nabla p_e|)$ and D_α .

(b) A transient decrease of $\max(j_\phi)$ is observed when $\max(|\nabla p_e|)$ increases (at $t = 0.332$ s and $t = 0.355$ s). A possible explanation here is that the increased collisionality (as the increase in $|\nabla p_e|$ is mainly due to an increase in n_e) reduces the bootstrap fraction of the edge current [5].

A more detailed comparison between the pressure driven current and j_ϕ measured by MSE is shown in figure 3. It shows j_ϕ based on the neoclassical calculation of the bootstrap current [6, 7]. Profiles are shown just after the ELM ($t = 0.347$ s), when the MSE measured j_ϕ is still high, and late in the ELM-free period when both the measured j_ϕ and $|\nabla p_e|$ have recovered ($t = 0.367$ s). It is clear that in both cases the neoclassical calculation yields a lower and more narrow peak in j_ϕ than that measured by MSE. This could be due to the assumptions made for the neoclassical calculation ($T_i = T_e$, $n_i = n_e$), the spatial resolution of the MSE diagnostic, However, it could also be possible neoclassical theory is no longer valid in the plasma edge during H-mode because $\rho_\theta \sim L_n$ (with ρ_θ the poloidal gyroradius and L_n the density gradient length).

Finally $\max(j_\phi)$ was plotted as a function of $\max(|\nabla p_e|)$, as is usually done for a stability plot (figure 4). To determine the stability boundary ELITE calculations were performed for 2 time points just before the first ($t = 0.343$ s) and last ($t = 0.383$ s) ELMs [8, 9]. This resulted in the 2 dashed lines on figure 4, indicating the ballooning boundary of the stability region. A peeling boundary was not found for these time points. To guide the eye a dotted line is added to the figure in the location were the peeling boundary is expected. It is observed that during the type III ELM phase of the discharge $\max(j_\phi)$ and $\max(|\nabla p_e|)$ are located in the area where the peeling boundary is expected (crosses). In the first long ELM free period $\max(j_\phi)$ and $\max(|\nabla p_e|)$ start near the peeling boundary, but then move towards the ballooning boundary: increasing $\max(|\nabla p_e|)$ and decreasing j_ϕ . At the ELM crash $\max(|\nabla p_e|)$ drops while $\max(j_\phi)$ keeps on rising, consequently getting close to the peeling boundary again. $\max(|\nabla p_e|)$ then quickly starts to increase, while $\max(j_\phi)$ drops, moving towards the ballooning boundary again. $\max(|\nabla p_e|)$ and $\max(j_\phi)$ subsequently increase, more or less following the ballooning boundary.

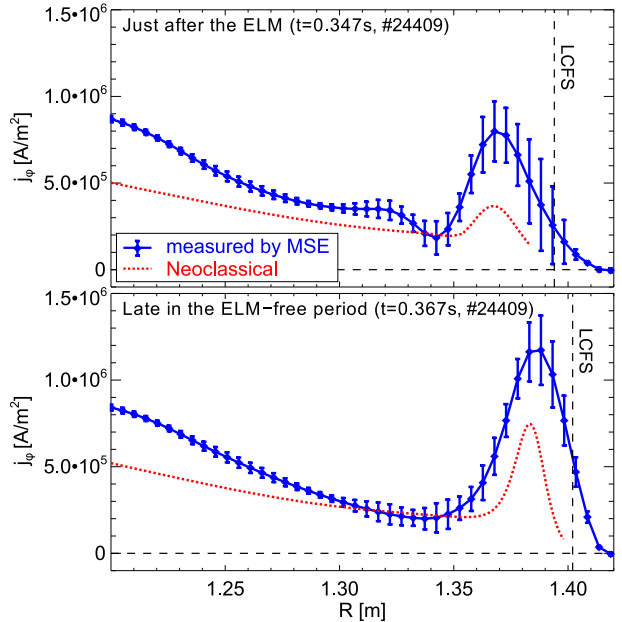


Figure 3: Comparison of j_ϕ measured by MSE and that based on the neoclassical bootstrap current.

The above results show the capability of MSE as tool for measuring the evolution of the edge j_ϕ in spherical tokamaks. This thanks to the large pitch angle and the fact that the E_r correction is small. The evolution of j_ϕ shows interesting behaviour that does not always seem to correlate with $|\nabla p_e|$. Neoclassical calculations of the bootstrap current typically result in lower values for edge j_ϕ than measured with MSE. Further and more detailed analysis on a wider variety of discharges will allow to evaluate the agreements and disagreements between the measured data, neoclassical calculations and stability codes. Also a new EBW (Electron Bernstein Waves) emission diagnostic is being constructed at MAST, designed specifically to measure the pitch angle in the edge and hence complement the MSE data[10].

This work was jointly funded by the United Kingdom Engineering and Physical Sciences Research Council and by the European Communities under the Contract of Association between EURATOM and CCFE. The views and opinions expressed herein do not necessarily reflect those of the European Commission.

References

- [1] M. F. M. de Bock, N. J. Conway, M. J. Walsh *et al* , “Ab initio modeling of the Motional Stark Effect on MAST”, *Review of Scientific Instruments*, vol. 79, no. 10, p. 10F524, 2008.
- [2] N. J. Conway, M. F. M. De Bock, C. A. Michael *et al* , “The MAST motional Stark effect diagnostic”, *Review of Scientific Instruments*, vol. To be published: proceedings 18th conference on High-Temperature Plasma Diagnostics, May 2010, 2010.
- [3] L. C. Appel, G. T. A. Huysmans, L. L. Lao *et al* , “A Unified Approach to Equilibrium Reconstruction”, in *33rd EPS Conference on Controlled Fusion and Plasma Physics* (ECA, ed.), vol. 30C, pp. P-2.184, EPS, 2006.
- [4] H. Meyer, C. Bunting, P. G. Carolan *et al* , “The structure, evolution and role of the radial edge electric field in H-mode and L-mode on MAST”, *Journal of Physics: Conference Series*, vol. 123, p. 012005, 2008.
- [5] D. M. Thomas, A. W. Leonard, T. H. Osborne *et al* , “The effect of plasma collisionality on pedestal current density formation in DIII-D”, *Plasma Physics an*, vol. 48, pp. A183–A191, 2006.
- [6] O. Sauter, C. Angioni, and Y. R. Lin-Liu, “Neoclassical conductivity and bootstrap current formulas for general axisymmetric equilibria and arbitrary collisionality regime”, *Physics of Plasmas*, vol. 6, no. 7, p. 2834, 1999.
- [7] O. Sauter, C. Angioni, and Y. R. Lin-Liu, “Erratum: §Neoclassical conductivity and bootstrap current formulas for general axisymmetric equilibria and arbitrary collisionality regime† [Phys. Plasmas 6, 2834 (1999)]”, *Physics of Plasmas*, vol. 9, no. 12, p. 5140, 1999.
- [8] H. Wilson, P. Snyder, G. Huysmans *et al* *Physics of Plasmas*, vol. 9, p. 1277, 2002.
- [9] P. Snyder, H. Wilson, and et al. *Physics of Plasmas*, vol. 9, p. 2037, 2002.
- [10] V. F. Shevchenko, M. F. M. D. Bock, S. Freethy *et al* , “2D EBW studies in MAST”, in *16th Joint Workshop on Electron Cyclotron Emission and Electron Cyclotron Resonance Heating*, Sanya, China, 2010.

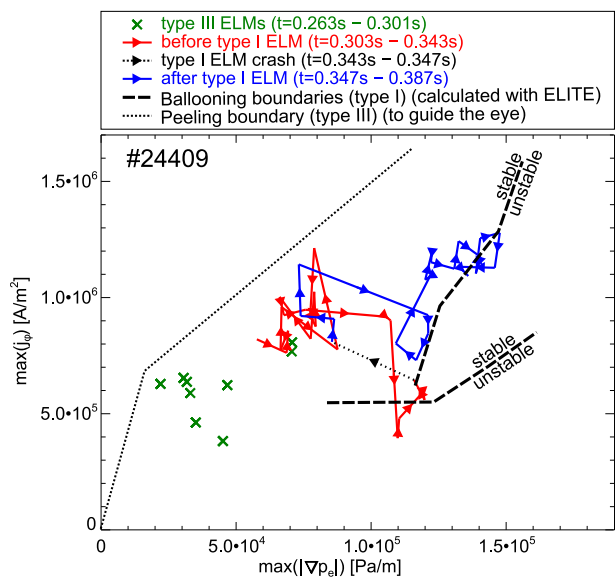


Figure 4: $\max(j_\phi)$ plotted versus $\max(|\nabla p_e|)$. This shows the evolution within the stable region.